On the design of a small scale tidal converter for long time deployment at sea

D. Alizzio, L. Gurnari, V. A. Nardi, M. Torresi, D. Coiro, S. Camporeale, P. Filianoti,

Abstract—**A scale model of a kite-like converter of tidal energy, the GEMSTAR, is designed to be installed at sea for a long term deployment. The aim of the experiment is to develope a digital twin with fault detection and isolation capabilities. To this aim, a fully-functional 1:10 scale of GEMSTAR is designed, starting from measurements of tidal currents in the site of installation. Several spots were investigated searching for the most suitable current profile. The paper describes the principal issues concerning operational functions and the choice of the physical parameters to monitor during the deployment through several sensors placed on board.**

Index Terms—**Tidal currents; energy converters; operative matching; 3D-scanning; computational fluid dynamics;**

I. Introduction

According to the Paris agreement, by 2030 at least 60% of electrical power will have to be produced by renewable sources. Therefore the average 6% 2019-2021 annual growth in renewable energies should double in 2022-2030 [1]. This comes in contrast with the fact that some mature technologies, such as hydroelectric power, could provide only a smaller fraction of the needed growth, opening the quest for yet unexplored production by previously neglected renewable sources. Following this path, the idea of harnessing energy from the sea dates back at least to the Roman era, when tidal rise and fall along rivers were exploited through tidal mills. Tidal energy generation is an attractive choice for its huge production potential, and some interesting features of marine currents, such as a good level of predictability (due to the regularity of astronomical effects) [2] and a reduced footprint in comparison to other renewable energies. Several studies assessed its production potential [3] and a 2004 report by Black and Veatch Consulting Ltd estimates a practical available energy production in the 10-30 TWh/year range for the sole United Kingdom [4].

A plethora of tidal current technologies aim to commercialization, and a vast scientific literature deals with the relevant topics in tidal current energy production, either from oceanic flows, river flows, or tide-induced motions of water. Technological solutions can be divided into [5]: hydrokinetic turbines on floating devices (either submerged or emerged), bottom-mounted hydrokinetic turbines (similar, in concept, to wind farms), and underwater kite-like devices equipped with hydrokinetic turbines.

Literature focuses upon different technological aspects in tidal energy production, for instance, in [6] a comparative study between a wave device (the Oyster) is compared to a tidal bottom-mounted turbine (the SeaGen) in terms of efficiency and overall carbon footprint. A wide economic analysis of tidal energies has been carried out in [7], focusing upon economical sustainability of floating devices. An interesting experimental study about a moored device has been performed in [8], although the device operated on battery for a limited amount of time (three days). In [9] attention is devoted to efficiency problem in presence of turbulence, relying upon real-World data to fed an improved BEM model. As outlined in [10], a recent trend in tidal energy research expands tidal energy schemes into wider coastal/estuarine management plans, stressing the multi-disciplinarity of research effort in the area. The interested reader can find some reviews of tidal energy literature and hotter topics in [5], [10]–[13].

Belonging to the kite-like category, the GEMSTAR [14], [15] is a kite-like submerged floating device (see Figure 1), tethered to the seabed through a flexible mooring cable, which produces energy by intercepting the tidal stream mechanical power through two symmetrical hydrokinetic turbines equipped with three composite blades. The system is able to align itself to the current direction change [2], by free rotation. GEMSTAR has been developed by non-profit applied research consortium SEAPOWER participated by University of Naples Federico II.

A series of advantages is offered by the GEMSTAR solution, such as decreased maintenance costs due to the flexibility in handling the system outside water, the absence of active rotating control parts and its self-aligning properties. Moreover, a performances comparison, carried out in [16] through simulations in a real-world scenario, highlights a total efficiency almost double than its closer competitor among selected technologies. A new deployment of a reduced scale model of the GEMSTAR, is being carried out in the stretch of sea in front of the Marine Energy Lab (RENEWMEL) along the Eastern side of the Strait of Messina [17]. The location is known due to the magnitude and regularity of the current velocity and therefore, is of great interest for energy production [18]. Namely,

D. A., L. G., V. A. N., and P. F. authors are with University Mediterranea of Reggio Calabria, Via dell'Università, 25, 89124 - Reggio Calabria, Italy email:{damiano.alizzio,luana.gurnari,vito.nardi,filianoti}@unirc.it

D. C. author is with University of Naples Federico II, Via Claudio 21, 80125 - Napoli, Italy email: domenico.coiro@unina.it

M. T. and S. C. authors are with Polytechnic of Bari, via Amendola 126/b, 70126 - Bari, Italy email:{marco.torresi,camporeale}@poliba.it

Digital Object Identifier:
https://doi.org/10.36688/ewtec-2023-567

Fig. 1. A render of the GEMSTAR model to be installed off the beach of Reggio Calabria.

Fig. 2. A map of the RENEW-MEL site in the Strait of Messina. The red point indicates the position of the laboratory.

the Strait of Messina has the highest resource value of tidal stream energy in the Mediterranean sea [19]. In particular, the maximum velocities recorded range between 1.8 m/s to more than 3 m/s [20], conveying a semi-diurnal pattern [21]. The potential production from tidal stream in the Strait of Messina are estimated in [16], and ranges up to 125 GWh/y, by considering only most accessible depths. The deployment of the GEMSTAR will be characterized by long-term operation of the device, focusing upon some problems such as the need for an active control of attitude, aiming to prevent cable twisting and to improve the alignment of the device with the current. Also, fault detection and isolation [22] and predictive maintenance techniques for the GEMSTAR will be developed and applied. Moreover, a critical issue, once the system is operational in the real sea environment for an enduring long period, is to guarantee a high efficiency level of the tidal turbines, for maintaining stable the energy production. Indeed, this performance is under the threat of marine biofouling, whose effects on tidal turbine systems are barely known neither quantified, except for a few numerical studies on the roughness effect due to biofouling presence on system components. The aim of this work is to illustrate various aspects and choices involved in the design of the small scale model. The paper is articulated as follows. Sect. II characterizes the marine currents in the site of installation. Sect. III fixes geometries and working parameters. Sect. IV exposes the analysis for the kinetic conversion. Sect. V analyzes power conversion, while Sect. VI gives an overview of the measurement architecture.

II. Characterization of the deployment site

Each site for harvesting tidal energy has its own characteristics, which must be investigated to estimate its potential productivity. Several studies have investigated the characteristics of tidal currents in the Strait of Messina, for example [23] and surveys by the Italian Hydrographic Institute [24]. Although a significant variability in current speed values is present, a general semi-diurnal pattern, due to tidal effects, can be identified, with four peaks a day. The site of installation is off the promenade of Reggio Calabria (see Figure 2), a city along the calabrian coast of the Strait of Messina. The alignment of the shoreline is SO-NE and the RENEW-MEL laboratory is close to the mouth of the Calopinace river (see Figure 3). There, the tidal currents are particularly non-homogeneous spatially, due to the vicinity of the coast, the shape of the seabed and the local orientation of the coast. For this reason, several current speed measurements had been carried out in different positions. To specify, over a year of measurement campaign have been conducted in the

positions named A, B and C (see Figure 3). Position

Fig. 3. Three hypothetical installation sites of the current energy converter, where the measurement campaign was conducted.

A, is the closest to the mouth of the Calopinace River. Measurements have been acquired locally through an Acoustic Wave and Current Profiler instrument, the Nortek AWAC AST 600kHz, from December 2020 to March 2021. The instrument was installed about at 7 m below the sea water level. The position of this installation site was chosen in order to investigate the influence of the river mouth on the speed and direction of the current. Position B, is the deepest location investigated. It was chosen in order to evaluate, along the water column, the variability of speed and direction of the current, in a position less affected by the presence of the coast. It was instrumented by the Nortek AWAC AST 600kHz, from April to November 2021, installed at 16 m below the s.w.l. Finally, location C is the most nearshore and, due to the particular conformation of the coast, is a sheltered site. It was instrumented by the Nortek AWAC AST 600kHz, from October to November 2020, at 6 m depth. To examine the spatial variability of the current, polar plots of several classes of current speed, for the three considered points have been carried out (see Figure 4). Whilst directions can be compared among different points, the occurrence of the same class of velocity in A, B and C may be not strictly comparable, due to the non-simultaneity of measurements in these three points. As we can observe in Figure 4, the most frequent current speed was registered at 2 m below the s.w.l. at the position A and it is between [0.5 - 0.75] m/s (see the green line). It is directed towards SSW and it occurred the 18 % of the time (*i.e.* 65 days in a year). It is followed by the the current speed included between [0.75 - 1] m/s and [1 - 1.25] m/s, directed towards SSW, that occur for 22 days and 15 days per year, respectively. The installation site B is characterized by current speeds between [0.5 - 0.75] m/s, registered at 4 m below the s.w.l., that occurs for 20 days per year and it is directed towards SW. Moreover, in both points A and B, predominates the ebb stream (*i.e.* the current flowing towards the Jonian sea). This current flows nearly parallel to the coast in B and inclined at about $40°$ in A. Point C is the nearest to the coast and is sheltered by a

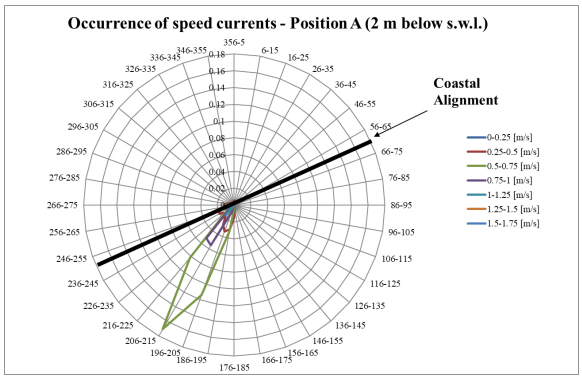

(a)

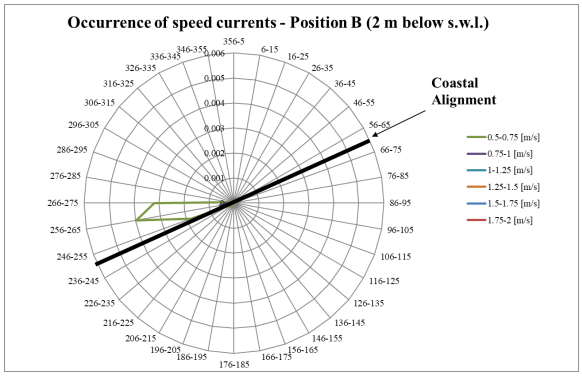

(b)

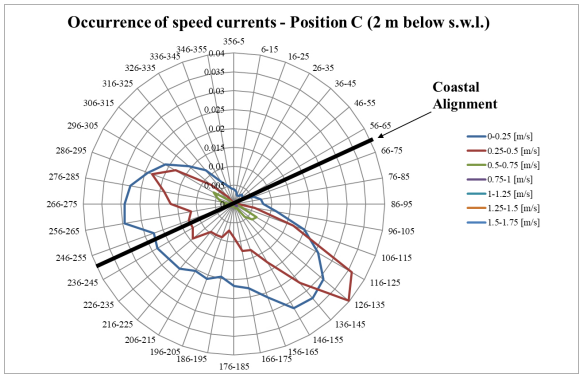

(c)

Fig. 4. Frequency of speed and direction of currents occurring in the three locations indicated in Figure 3.

pronouncement of the coast in the southern part. The directions of current occur almost perpendicular to the shoreline acting similarly to the rip currents induced by wave breaking. Figure 5 shows a typical current profile along the z-axis, for the three considered positions (A, B and C). The maximum velocity occurs near 2 m below the sea surface, in both point A and C, while point B shows highest velocity value at water surface. In position B, the maximum speed occurs at the sea surface. The installation depth has been chosen at 2m below s.w.l., as we can see in Figure 4, deep enough to ensure the navigation safety and shallow enough to intercept higher currents speed.

The absence of flood stream (i.e. the current flowing towards the Tyrrenian Sea) evidenced in Figure 5 is confirmed also in Figure 6, which shows a 4 days time history of the current speed in A (the blue line). During the time intervals when we should have the

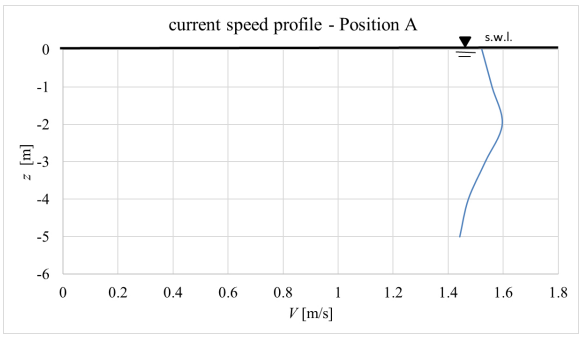

(a)

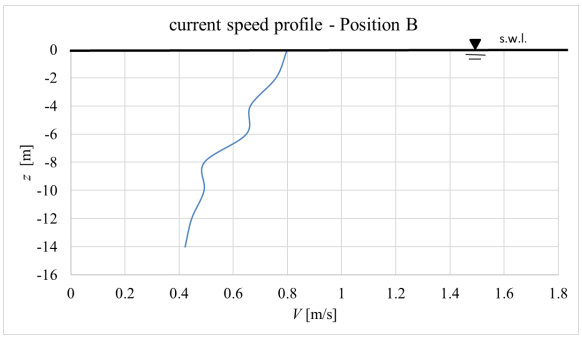

(b)

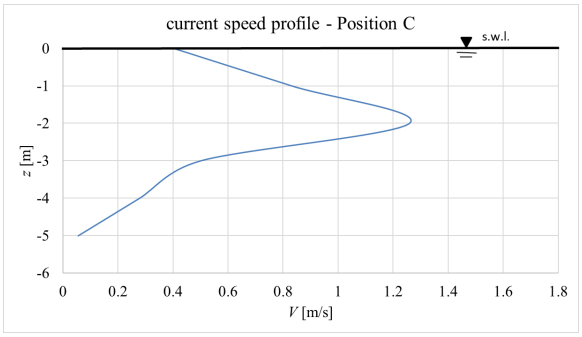

(c)

Fig. 5. current speed profile in the three locations indicated in Figure 3.

flood stream, we observe instead a constant ebb flow of about 0.6 m/s. These secondary flows, moving in the opposite direction in respect to the main stream, are frequent near the shores, and are commonly known as "bastards".

In light of the above analysis, the most suitable installation site for the GEMSTAR device appears to be the position A, the closest to the mouth river considering as design speed 0.9 m/s, equal to the average value of the marine current speed, during the observation period at the given quote. An harmonic analysis of the three flow current records was also performed with the aim to extend the predictions to a yearly period. The current speed records have been filtered out subtracting their constant components, and processed through the "T-tide" tool in MATLAB environment [25], [26]. This is an useful tool for harmonic analysis of tidal records and for comparison purposes with values available in the Literature [16]. Starting from recorded values or tide atlas values, this tool can provide the spectral composition of gravitational constituents leading the input signal. Table I reports

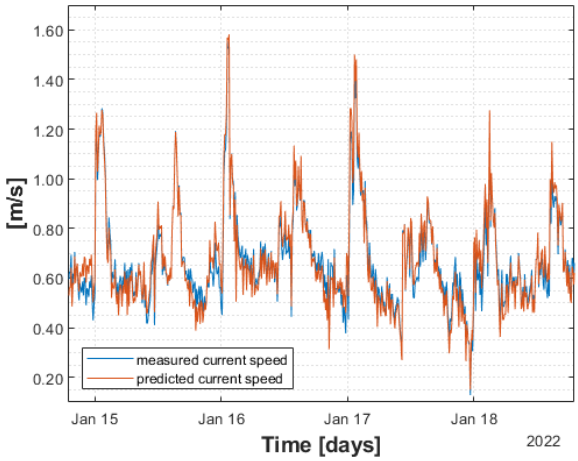

Fig. 6. Time history of the current speeds in the location A of Figure 3: comparison between predicted and measured current speed.

the principal 20 constituents for the data records, in order of their amplitudes. A prediction of expected flow speed was computed starting from the detected constituents. The orange plot in Figure 6 indicates the flow speed prediction. The prediction reveals an underestimation of the flow speed by about 13%.

TABLE I
SUMMARY OF HARMONIC ANALYSIS RESULTS: POSITION A

Constituent name	Freq. cph	Period h	Amplitude m/s	Phase °
'*MM'	0.0015	661.2882	0.0794	60.66
'*M2'	0.0805	12.4206	0.0544	37.21
'*MSF'	0.0028	354.3712	0.0385	76.45
'*K1'	0.0418	23.9345	0.0263	310.05
'*MN4'	0.1595	6.2692	0.0242	209.85
'*MK3'	0.1223	8.1771	0.0201	38.05
'*NO1'	0.0403	24.8332	0.0195	221.78
'*S2'	0.0833	12.0000	0.0171	74.88
'*M4'	0.1610	6.2103	0.0161	181.28
'*MO3'	0.1192	8.3863	0.0158	136.64
'*MS4'	0.1638	6.1033	0.0145	256.27
'*MU2'	0.0777	12.8718	0.0137	260.66
'*UPS1'	0.0463	21.5782	0.0121	164.67
'*N2'	0.0790	12.6584	0.0118	338.62
'*2Q1'	0.0357	28.0062	0.0117	28.97
'*Q1'	0.0372	26.8684	0.0113	160.43
'*L2'	0.0820	12.1916	0.0108	108.83
'*ETA2'	0.0851	11.7545	0.0098	90.51
'*SN4'	0.1623	6.1602	0.0097	226.94
'*M3'	0.1208	8.2804	0.0090	218.49

III. THE TURBINE ROTOR GEOMETRY AND WORKING PARAMETERS

A vertical view of the positioning of the GEMSTAR device during functioning is shown in Figure 7. The optimal device vertical position z is where the highest values of current speed occurs, along the vertical axis of the installation site. Moreover, the vertical position of the device effectively depends on the buoyancy/drag forces compound. The more the current speed increases, the more the device goes deeper. Referring to the Figure 7, the minimum quote z_{min} represents the idle position of the system (*i.e.* in absence of current). The value of z_{min} can be assumed equal to the sum of half the height of the maximum expected wave,

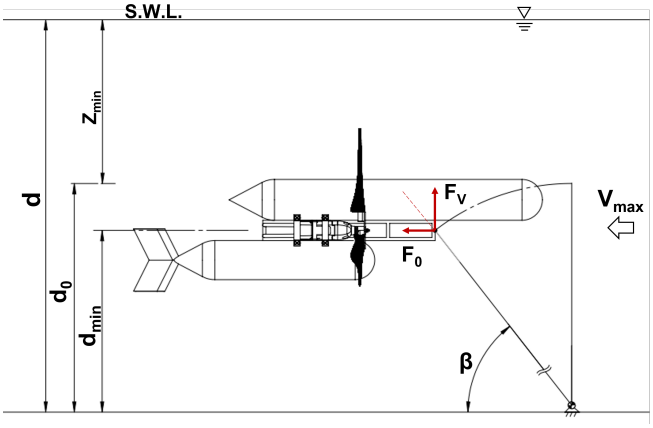

Fig. 7. A vertical view of the GEMSTAR device during operational.

the absolute maximum amplitude of tide and a safety distance (*i.e.*, one and half the rotor radius R). Thus, the working depth of the device $d_0 - d_{min}$, depends on the angle of inclination β through the following condition:

$$\beta = \arcsin\left(1 - \frac{d_0 - d_{min}}{d_0}\right). \tag{1}$$

The angle β_{min} depends on the tension applied to the mooring line:

$$\beta_{min} = \arctan\left(\frac{F_V}{F_{0,max}}\right), \tag{2}$$

where F_V is the buoyancy force and $F_{0,max}$ is practically coincident with the sum of the thrusts exerted by the two rotors during the current with the maximum speed. Table II summarizes the geometrical configuration of the system subjected to a V_{max} = 1.6 m/s. To obtain this working configuration, we have to calculate $F_{0,max}(V_{max})$ and fix the value of F_V, in order to obtain the given β_{min}.

TABLE II
GEMSTAR LAYOUT

$\boldsymbol{d}$	m	7
$\boldsymbol{z_{min}}$	m	2
$\boldsymbol{d_0 - d_{min}}$	m	0.5
$\boldsymbol{\beta_{min}}$	deg	65°

Applying the Blade Element Momentum Theory (BEMT), the rotor performances were studied, and the characteristic curves generated. Under the action of the typical current speeds occurring in the installation site, the theoretical power and the thrusts of the rotor have been evaluated during the deployment period. These results represent the input parameters for the design of the energy converter device. Considering the distribution of velocity in the installation site, a rotor diameter of 1.2 m was choosen, in order to guarantee the rotation of the blades at low speeds. The actual blade geometry was accurately checked through laser scanning. An Artec EVA 3D-scanner was used for this purpose, having an accuracy of ±0.1 mm. The blade model was subsequently sliced along its radial axis and 23 sections of the hydrofoil were extracted. The leading and trailing edges were detected for each slice and, thus, measurements of the foil chord length c and pitch angle α have been drawn. A further match with the physical model of the blade has returned a maximum error on the chord length equal to ±0.09 mm. Figure 8 shows the physical blade (a) and the mesh for its respective 3D reconstruction (b). The blades will be recovered and scanned periodically to evaluate the influence of biofouling. Subsequently, Computational Fluid Dynamic (CFD) simulations on the scanned real surface will be conducted, and the new performance will be compared to the previous ones to track and quantify the biofouling effect on rotor performances.

IV. The Kinetic Energy Captured by the Rotor

Once the rotor blade were scanned and the mesh slices were normalized with respect to their own chord length, the drag and lift coefficients were estimated, by means of the Open Source code X-Foils, which uses a simple linear-vorticity stream function panel method, under the hypothesis of inviscid fluid. Applying the Blade Element Momentum Theory to the rotor reconstructed from the detected sections, the characteristic curves of the turbine were carried out. The hydrodynamic thrusts of the rotors were calculated with respect to the rotational speed of the rotor itself and parameterized with respect to the speed of the fluid current. In the same way, the theoretical mechanical power intercepted by the rotor was calculated as a function of the rotational speed n and parameterized with respect to the fluid current velocity. These curves permit also to estimate the maximum torque curves and the maximum catchable power as a function of the current speed V. Figures 9 and 10 show the theoretical torque and mechanical power available on the machine axis, respectively.

The family of curves is drawn for several values of the current speed, ranging from 0.5 m/s to 1.75 m/s, at an interval of 0.25 m/s. The black dashed line joins the maxima of each curve. Similarly, Figure 10 represents the power at the hub of the rotor, as a function of the rotational speed n. The black dashed line has the same meaning as in Figure 9, and it can be well represented by a linear relationship in the plane (n, V):

$$\boldsymbol{n} = 72.7\boldsymbol{V}, \tag{3}$$

where $\boldsymbol{n}$ denotes the angular speed of the turbine rotor in [rpm] and $\boldsymbol{V}$ the water speed in [m/s]. This relationship is useful to implement control strategies aiming at maximizing the power production. The torque $\boldsymbol{T_0}$ exerted by a current of given velocity $\boldsymbol{V}$, when the rotor is arrested is shown in Figure 11 and it can be interpolated by the quadratic relationship:

$$\boldsymbol{T_0} = 18.7\boldsymbol{V}^2, \tag{4}$$

It is useful to determine the minimum speed of the current able to start the rotation.
Considering the maximum power captured by each rotor, shown in Figure 10, two electrical generators with rated power of 1.4 kW are chosen. The maximum thrust $F_{0,max}$ exerted by a current with V_{max} = 1.6 m/s is equal to 1014 N. Considering Eq. 2, the F_V

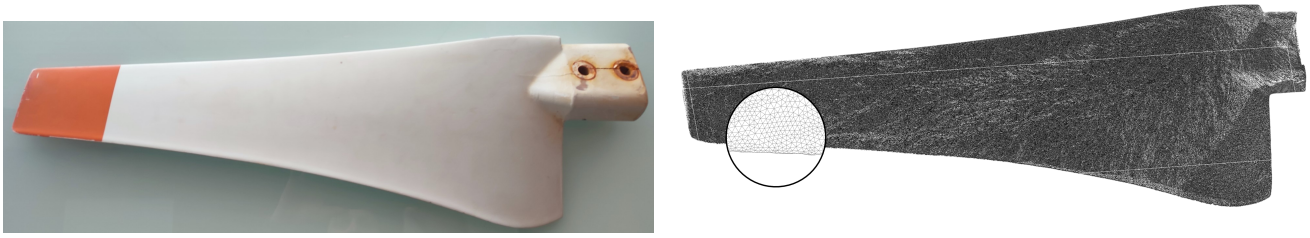

((a)) ((b))

Fig. 8. GEMSTAR a) rotor blade and b) mesh captured by the 3D-scanner.

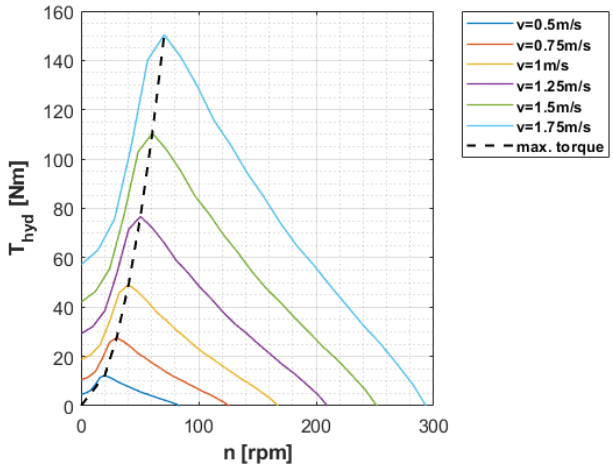

Fig. 9. Theoretical torque of the turbine rotor as a function of the rotational speed n, for several values of the current speed.

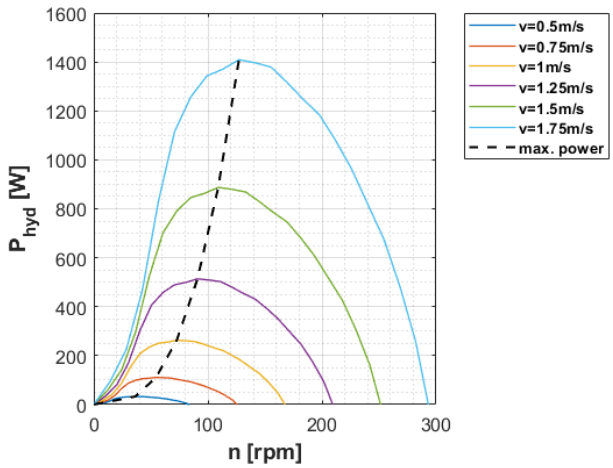

Fig. 10. Theoretical mechanical power of the turbine rotor

must be equal to 2940 N, to maintain the angle β of inclination of the mooring line at the desidered value of 65°. The mechanical power captured from the stream will then be conveyed to two Brushless Direct Current (BLDC) electric generators mounted downstream the rotor shafts. Brushless direct current (BLDC) permanent magnet machines are a popular choice for renewable energy generation, owing to the fact they offer several advantages in terms of durability, wide operating range, high efficiency, low maintenance, and power density [27]. This is mainly due to the lack of

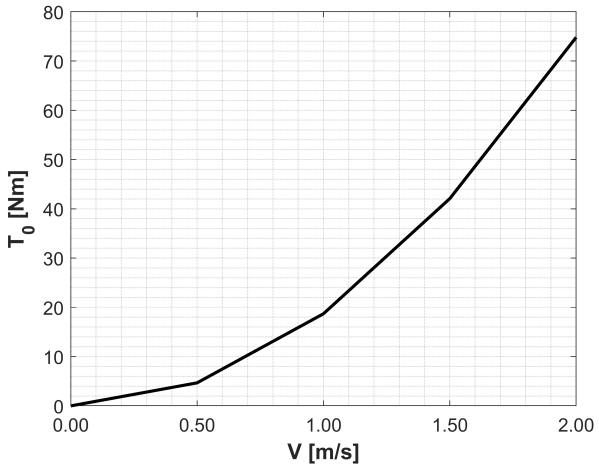

Fig. 11. Rotor starting torque as function of the current speed V.

moving contact elements (brushes) whose abrasion is the main cause of fault in conventional DC generators followed by commutation sparks [28]. The experimental apparatus described in this work uses two Nanotec DC80 BLDC motors as power generators. Therefore, no characterization data of the DC80 as a generator are available. A proper characterization procedure needs to be applied, in order to draw the required mechanical power versus angular speed, and electrical power versus angular speed curves, on varying the electrical load. On the other hand, axis torque versus electrical load measurements bring up information on the cogging torque of the DB80 as generator. An ad hoc test bed has been developed. It includes a DC motor which provides the generator with a known mechanical power through a rigid joint, and an electrical load for the dissipation of generated electrical power. The test bed is equipped with the sensors to measure speed of the driving motor/generator system, and both current and voltage applied to the load. During the characterization procedure, the system is driven at different velocity set-points, using a closed loop feedback control aimed at obtaining a stable velocity and a smooth transient behaviour.

V. The Mechanical Efficiency of the System

The quota of tidal power stream which can be captured has been evaluated through the BEM. Several control strategies can be exploited for maximizing the power production. An attractive choice is velocity

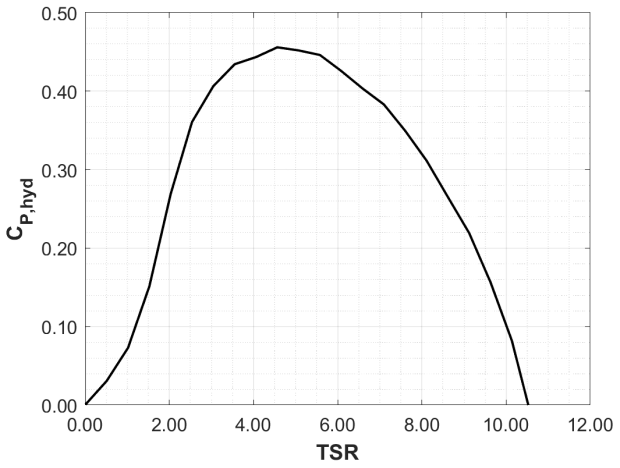

Fig. 12. Expected hydraulic power coefficient $c_{P,hyd}$ for one rotor of the GEMSTAR kite converter

control: power is produced while holding a constant rotational speed by reducing the torque, which is picked up, and increasing the rotational speed of the generator [29]. This approach makes the rotor work in a flux-wakening condition [2]. Torque drive is carried out through a speed multiplier 1:20, in order to meet electrical characteristics of the generator. An estimation of power loss in a stationary regime during drive has been provided, by considering the loss contribution of each drive part. Let P_{TOT}, be the reference tidal power referred to the undisturbed water velocity, V, and passing through the area S swept by the rotors, P_{hyd} the hydraulic power available at the rotor hub, P_m the mechanical power available to the generator shaft, and P_{el} the electrical power which can be obtained, the following efficiency coefficients have been defined:

$$P_{EL} \equiv \eta_{el}\eta_m c_{P,hyd} P_{TOT} \equiv c_P P_{TOT}, \tag{5}$$

where $\eta_{el} \equiv \frac{P_{EL}}{P_M}$, is the electrical efficiency of the generator, $\eta_m \equiv \frac{P_M}{P_{HYD}}$, is the mechanical efficiency of power drive and $c_{P,hyd} \equiv \frac{P_{HYD}}{P_{TOT}}$, hydraulic power coefficient of rotors. Overall,

$$c_p \equiv \eta_{el}\eta_m c_{P,hyd}, \tag{6}$$

is the power coefficient of the whole conversion chain. The power coefficient c_p, along with its factors, depends on rotational speed. The hydraulic power coefficient can be expressed as:

$$c_{P,hyd} \equiv \frac{P_{HYD}}{0.5\rho S V^3} \tag{7}$$

as the ratio between hydraulic power intercepted by the rotor and the reference power of the tidal current $P_{TOT} = 0.5\rho S V^3$. In general, $c_{P,hyd}$ is expressed as a function of the Tip Speed Ratio TSR:

$$TSR \equiv \frac{\omega R}{V}, \tag{8}$$

where ω represents the rotor angular velocity. Figure 12 shows expected $c_{P,hyd}$ coefficient values for one of the two rotors of the GEMSTAR device as a function of TSR.

In order to find mechanical efficiency coefficients, torque curves and hydraulic power curves found through Blade Elements Momentum Theory (BEMT) have been considered. Mechanical torque which is available to the shaft of the generator is the difference between hydraulic torque available at the rotor and the hydraulic torque dissipated along the transmission $T_{HYD}(n,V) - T_D(n)$. Namely, it has been necessary to take into account the most important mechanical loss factors related to moving parts. Dissipated torque can be evaluated as:

$$\begin{aligned} T_D(n) = T_{D,gearbox}(n) + \\ T_{D,bearings}(n) + T_{D,bellow\,seals}(n), \end{aligned} \tag{9}$$

i.e., the sum of torque dissipated by the gear box, rolling bearings, and bellow axial seals. The speed multiplier power efficiency was assumed to be equal to 0.97 as declared by the manufacturer.
Regarding on the righ-hand term of the Eq. 9, the torque $T_{D,gearbox}$ dissipated by the gear box was assumed taking into account the nominal efficiency value of 97%, as described by the manufacturer. As regard to the power dissipated by the rolling bearings, the torque absorbed has been calculated as reported in [30]. In particular, the following model for calculating the bearings frictional moment has been used:

$$\begin{aligned} T_{D,bearings}(n) = \\ T_{rf}(n) + T_{sf}(n) + T_{bs}(n), \end{aligned} \tag{10}$$

where M_{rf} is the rolling frictional moment, M_{sf} represents the sliding frictional moment and M_{bs} is the frictional moment of the two bearings seals. The third addend of the right-hand member of the Eq. [9] is the torque dissipated by bellow seals, computed as:

$$\begin{aligned} T_{D,bellow\,seals}(n) = \\ \eta_k \frac{D_m}{4} F_{preload} + K(n), \end{aligned} \tag{11}$$

where η_k is the friction coefficient adopted for the bellow seals sliding surfaces, acting on its average diameter D_m, and $F_{preload}$ is the nominal pre-load force for the seal locking. The dynamical contribution $K(\omega)$ depends on rotational speed and it has been considered negligible due to the low relative speed of the bellows friction surfaces. The friction coefficient has been considered both in static (equal to 0.51) and dynamic (equal to 0.23) conditions in a stationary regime. Static friction coefficient value was used to determine the turbine starting torque without any electrical load. The ratio between mechanical power and hydraulic power were used to estimate mechanical efficiency coefficient in stationary conditions, at different rotational velocities and different current speeds. Further experimental verification will be set up to verify this estimation. Figure 13 depicts mechanical efficiency values. Finally, the required starting torque value of 1.53 Nm relative to the rotor axis was obtained adding the nominal starting torque of the electric generator without any electrical load. From the hydrodynamic interpolation presented in Figure 11 and by relationship 4, the cut-in speed value

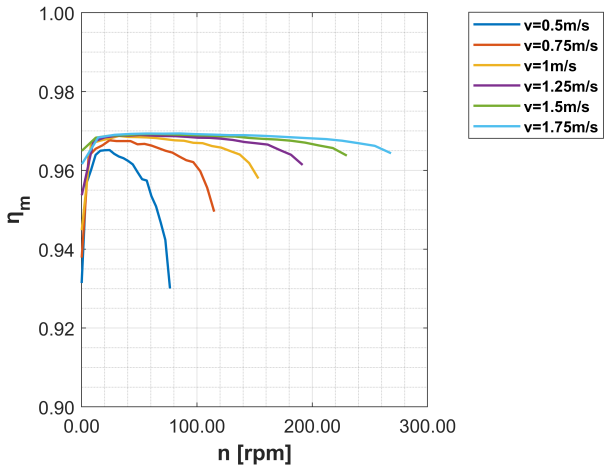

Fig. 13. Expected mechanical efficiency η_m of the GEMSTAR power transmission.

of 0.2859 m/s was estimated.

VI. Data collection and system control

Data collection serves three main purposes: power production management and optimization [31], system monitoring (including the crucial task of conversion efficiency estimation) and attitude control. Design of hardware and software for data collection has been performed accounting a series of criteria, namely:

- soft real-time monitoring;
- control capabilities;
- logging of data in a flexible format;
- low-cost architecture for floodable parts;
- ease of reconfiguration.

Each of the above-mentioned purposes relies upon the collection of some measurement, which are processed by a Raspberry Pi-based embedded unit (whose scheme is reported in figure 14) and are encapsulated in MQTT packets to be sent onshore over a TCP/IP network. More in detail, power production management and optimization require instant knowledge of power production onboard and turbines rotational speeds, leading to the need to measure both current and tension produced by the generators and the signals of the encoders embedded in the generators. Load management will follow a maximum power point tracking logic, with the aim to maximize power conversion efficiency. Attitude control has two main goals: preventing cable twisting and improving the alignment of the GEMSTAR with current, maximizing power production. For this reason, both relative direction and relative speed of sea current are measured through sensors installed on the device, while unperturbed current direction and speed are measured through an ADCP installed near the device, in the undisturbed field. Furthermore, system attitude (through MEMS [32] gyroscopes, accelerometers, and compasses sensors) and cable tension (using a load cell) are measured. In addition, an onboard pressure sensor will provide the device quote. Actuation will rely on generators, firstly by selectively slowing down one

TABLE III
Sampling frequencies of different measurements.

Measurement	Frequency (Hz)
IMU measurements	1
Power (voltage and current)	50
Current angles	1
Generators speed	2
Flooding sensors	0.1

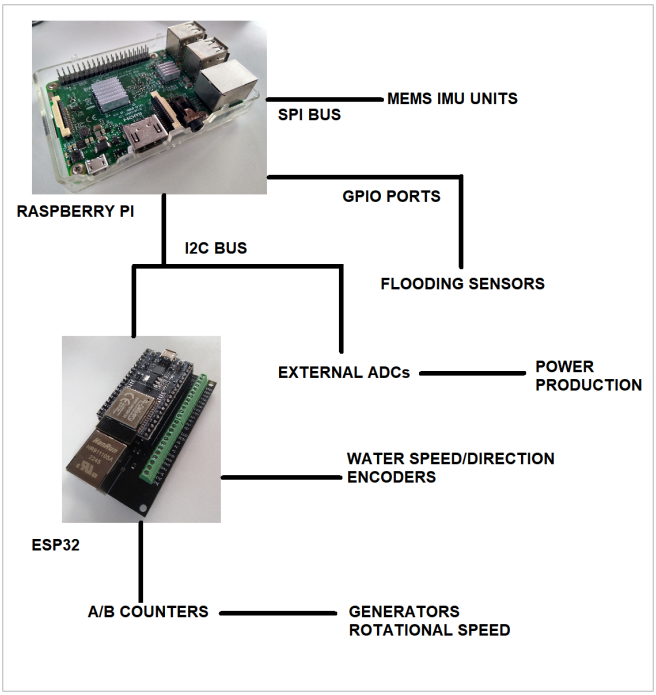

Fig. 14. A schema of the embedded data units onboard.

of the turbines through load management, secondly by switching generators operating regime to motor one. System monitoring will exploit all the mentioned measurement along with flooding sensors within the lower tank of the GEMSTAR. It will also provide the inputs for a digital twin [33] of the GEMSTAR, with fault detection and isolation capabilities. All of the three purposes of data collection may benefit from the knowledge of system dynamical model. However, some of its parameters, e.g., inertia matrix, are hard to determine with the required accuracy. Therefore, some parameters necessary for system monitoring and attitude control need to be identified via an ad hoc system identification procedure which will exploit gathering experimental data. Model-predicted behaviour will be matched against measured behaviour of the device, in order to validate the model. Table III summarizes both measurements and their relevant sampling frequency.

VII. Conclusions

This work illustrates the design concepts and preliminary work done for the long-term deployment of an underwater kite for power generation from tidal streams, in the stretch of sea facing the RENEW-MEL laboratory, in the Strait of Messina. The characterization of the site is still in course but has already allowed to fix the preliminary design of kite and turbines geometry. Each element of the power conversion chain

has been characterized, or a proper characterization procedure has been identified. The experiment will firstly allow for the attitude control of the device, with a close connection to energy production optimization, also through a proper electrical load management. Alongside, a digital twin of the device will be developed with fault detection and isolation capabilities. Long-term deployment will allow the study of biofouling effects on system efficiency, for which a proper procedure has been designed. Going beyond previous works, the long-term deployment is meant to be a necessary step in the path towards commercial use of tidal energy, while the required cross-disciplinary effort is expected to produce results of interest in several research fields.

REFERENCES

[1] P. Bojek, "Renewable electricity," 2022.

[2] D. P. Coiro, G. Troise, N. Bizzarrini, and G. Lazzerini, "Gemstar: A tethered system for tapping tidal currents energy," in *The 29th International Ocean and Polar Engineering Conference*. OnePetro, 2019.

[3] L. Blunden and A. Bahaj, "Tidal energy resource assessment for tidal stream generators," *Proceedings of The Institution of Mechanical Engineers Part A-journal of Power and Energy - PROC INST MECH ENG A-J POWER*, vol. 221, 03 2007.

[4] B. . V. ltd, "Carbon Trust Foreword to UK Tidal Current Resource and Economics Study," Carbon trust, Tech. Rep., 6 2011.

[5] S. B. Elghali, M. Benbouzid, and J. F. Charpentier, "Marine tidal current electric power generation technology: State of the art and current status," in *2007 IEEE International Electric Machines & Drives Conference*, vol. 2. IEEE, 2007, pp. 1407–1412.

[6] S. Walker and R. Howell, "Life cycle comparison of a wave and tidal energy device," *Proceedings of the Institution of Mechanical Engineers, Part M: Journal of Engineering for the Maritime Environment*, vol. 225, no. 4, pp. 325–337, 2011. [Online]. Available: https://doi.org/10.1177/1475090211418892

[7] C. Johnstone, D. Pratt, J. Clarke, and A. Grant, "A techno-economic analysis of tidal energy technology," *Renewable Energy*, vol. 49, pp. 101–106, 2013, selected papers from World Renewable Energy Congress - XI. [Online]. Available: https://www.sciencedirect.com/science/article/pii/S0960148112000651

[8] B. Guo, D. Wang, J. Zhou, W. Shi, and X. Zhou, "Performance evaluation of a submerged tidal energy device with a single mooring line," *Ocean Engineering*, vol. 196, p. 106791, 2020. [Online]. Available: https://www.sciencedirect.com/science/article/pii/S0029801819308911

[9] L. Perez, R. Cossu, A. Grinham, and I. Penesis, "An investigation of tidal turbine performance and loads under various turbulence conditions using blade element momentum theory and high-frequency field data acquired in two prospective tidal energy sites in australia," *Renewable Energy*, vol. 201, pp. 928–937, 2022. [Online]. Available: https://www.sciencedirect.com/science/article/pii/S0960148122016524

[10] D. Khojasteh *et al.*, "A large-scale review of wave and tidal energy research over the last 20 years," *Ocean Engineering*, vol. 282, p. 114995, 2023. [Online]. Available: https://www.sciencedirect.com/science/article/pii/S0029801823013793

[11] M. Vikas, S. Rao, and J. K. Seelam, "Tidal energy: a review," in *Proceedings of International Conference on Hydraulics, Water Resources and Coastal Engineering (Hydro2016)*, 2016.

[12] A. Roberts, B. Thomas, P. Sewell, Z. Khan, S. Balmain, and J. Gillman, "Current tidal power technologies and their suitability for applications in coastal and marine areas," *Journal of Ocean Engineering and Marine Energy*, vol. 2, pp. 227–245, 2016.

[13] S. P. Neill, K. A. Haas, J. Thiébot, and Z. Yang, "A review of tidal energy—resource, feedbacks, and environmental interactions," *Journal of Renewable and Sustainable Energy*, vol. 13, no. 6, 2021.

[14] D. Coiro, G. Troise, F. Scherillo, A. De Marco, G. Calise, and N. Bizzarrini, "Development, deployment and experimental test on the novel tethered system gem for tidal current energy exploitation," *Renewable Energy*, vol. 114, pp. 323–336, 2017, wave and Tidal Resource Characterization. [Online]. Available: https://www.sciencedirect.com/science/article/pii/S0960148117300502

[15] D. P. Coiro, G. Troise, and N. Bizzarrini, "Experiences in developing tidal current and wave energy devices for mediterranean sea," *Frontiers in Energy Research*, vol. 6, 2018. [Online]. Available: https://www.frontiersin.org/articles/10.3389/fenrg.2018.00136

[16] D. Coiro, G. Troise, T. Ciuffardi, and G. Sannino, "Tidal current energy resource assessment: the strait of messina test case," in *2013 International Conference on Clean Electrical Power (ICCEP)*. IEEE, 2013, pp. 213–220.

[17] R. Morello, C. De Capua, P. Filianoti, and M. Lugara, "A research laboratory for coastal and sea water pollution monitoring," vol. 2016-January, 2016, pp. 40–43. [Online]. Available: https://www.scopus.com/inward/record.uri?eid=2-s2.0-85045436567&partnerID=40&md5=11561a866cb7ded7e9ba70fc9286aedf

[18] P. G. Filianoti and L. Gurnari, "A field experiment on wave forces on an energy-absorbing breakwater," *Energies*, vol. 13, no. 7, p. 1563, 2020.

[19] T. H. Soukissian, D. Denaxa, F. Karathanasi, A. Prospathopoulos, K. Sarantakos, A. Iona, K. Georgantas, and S. Mavrakos, "Marine renewable energy in the mediterranean sea: Status and perspectives," *Energies*, vol. 10, no. 10, 2017. [Online]. Available: https://www.mdpi.com/1996-1073/10/10/1512

[20] T. El-Geziry, I. Bryden, and S. Couch, "Environmental impact assessment for tidal energy schemes: an exemplar case study of the strait of messina," *Journal of Marine Engineering & Technology*, vol. 8, no. 1, pp. 39–48, 2009.

[21] A. Cucco, G. Quattrocchi, A. Olita, L. Fazioli, A. Ribotti, M. Sinerchia, C. Tedesco, and R. Sorgente, "Hydrodynamic modelling of coastal seas: the role of tidal dynamics in the messina strait, western mediterranean sea," *Natural Hazards and Earth System Sciences*, vol. 16, no. 7, pp. 1553–1569, 2016.

[22] E. D'Amato, C. De Capua, P. F. Filianoti, L. Gurnari, V. A. Nardi, I. Notaro, and V. Scordamaglia, "Ukf-based fault detection and isolation algorithm for imu sensors of unmanned underwater vehicles," in *2021 International Workshop on Metrology for the Sea; Learning to Measure Sea Health Parameters (MetroSea)*. IEEE, 2021, pp. 371–376.

[23] D. P. Coiro, G. Troise, T. Ciuffardi, and G. Sannino, "Tidal current energy resource assessment: The strait of messina test case," in *2013 International Conference on Clean Electrical Power (ICCEP)*, 2013, pp. 213–220.

[24] M. Massi, E. Salusti, and C. Stocchino, "On the currents in the strait of messina." *Il Nuovo Cimento*, vol. C 2, p. 543–548, 09 1979.

[25] R. Pawlowicz, B. Beardsley, and S. Lentz, "Classical tidal harmonic analysis including error estimates in matlab using t-tide," *Computers Geosciences*, vol. 28, no. 8, pp. 929–937, 2002. [Online]. Available: https://www.sciencedirect.com/science/article/pii/S0098300402000134

[26] D. Codiga, "Unified tidal analysis and prediction using the utide matlab functions," 09 2011.

[27] N. Milivojevic, M. Krishnamurthy, A. Emadi, and I. Stamenkovic, "Theory and implementation of a simple digital control strategy for brushless dc generators," *IEEE Transactions on Power Electronics*, vol. 26, no. 11, pp. 3345–3356, 2011.

[28] Z. Zhang, Y. Yan, S. Yang, and Z. Bo, "Development of a new permanent-magnet bldc generator using 12-phase half-wave rectifier," *IEEE Transactions on Industrial Electronics*, vol. 56, no. 6, pp. 2023–2029, 2009.

[29] Z. Zhou, M. Benbouzid, J.-F. Charpentier, F. Scuiller, and T. Tang, "Developments in large marine current turbine technologies – a review," *Renewable and Sustainable Energy Reviews*, vol. 71, pp. 852–858, 2017. [Online]. Available: https://www.sciencedirect.com/science/article/pii/S1364032116311698

[30] "The skf model for calculating the frictional moment." [Online]. Available: https://www.skf.com/binaries/pub12/Images/0901d1968065e9e7-The-SKF-model-for-calculating-the-frictional-moment_tcm_12-299767.pdf

[31] G. Fulco, F. Ruffa, M. Lugarà, P. Filianoti, and C. de Capua, "Automatic station for monitoring a microgrid," 2020, pp. 309–314. [Online]. Available: https://www.scopus.com/inward/record.uri?eid=2-s2.0-85096747988&partnerID=40&md5=3f28b31bc67342be51ce6cf48c7c8d88

[32] E. D'Amato, V. A. Nardi, I. Notaro, and V. Scordamaglia, "A particle filtering approach for fault detection and isolation of uav imu sensors: Design, implementation and sensitivity analysis," *Sensors*, vol. 21, no. 9, 2021. [Online]. Available: https://www.mdpi.com/1424-8220/21/9/3066

[33] F. Ruffa, M. Lugarà, G. Fulco, D. Alizzio, F. Lo Savio, and C. De Capua, "Prognostic health management using ir thermography: The case of a digital twin of a niti endodontic file †," *Sensors*, vol. 23, no. 9, 2023. [Online]. Available: https://www.scopus.com/inward/record.uri?eid=2-s2.0-85159153535&doi=10.3390%2fs23094296&partnerID=40&md5=4a1d9fe519e099a4c646bad3cc62d52a